ACS central science

http://pubs.acs.org/journal/acscii

Research Article

Tuning Single-Polymer Growth via Hydrogen Bonding in Conformational Entanglements

Susil Baral,[⊥] Chunming Liu,*[,⊥] Xianwen Mao, Geoffrey W. Coates, and Peng Chen*

Cite This: *ACS Cent. Sci.* 2022, 8, 1116−1124

Read Online

ACCESS | Metrics & More | Article Recommendations | Supporting Information

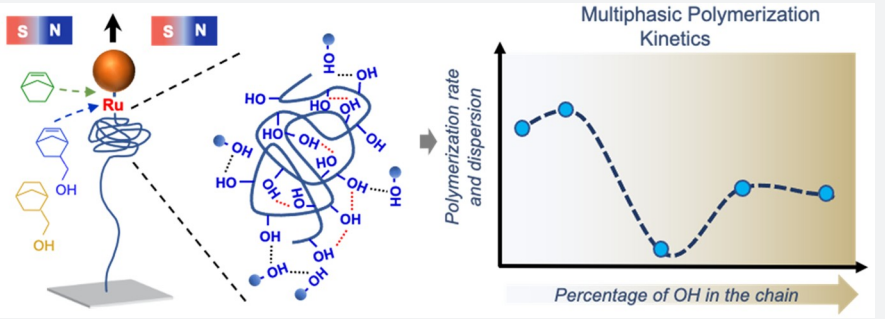

ABSTRACT: Synthetic polymers have widespread applications in daily life and advanced materials applications. Making polymers efficiently and controllably is highly desired, for which modulating intramolecular and intermolecular interactions have been an effective approach. Recent real-time single-polymer growth studies uncovered nonequilibrium conformational entanglements that form stochastically under living polymerization conditions and which appear to plausibly play key roles in controlling the polymerization kinetics and dispersion. Here, using magnetic tweezers measurements, we study the real-time polymerization dynamics of single polynorbornene-based polymers in which we systematically tune the hydrogen-bonding interactions by titrating the OH content in the monomers and the formed polymers during ring opening metathesis polymerization. Using norbornenes with and without a hydroxyl group and a nonreactive monomer analogue, we show that intrachain and intermolecular hydrogen bonding compete, and both alter the microscopic properties of the nonequilibrium entanglements, leading to surprising multiphasic dependences of polymerization dynamics on the polymer's OH content. We further formulate a simple model to rationalize quantitatively the observed multiphasic behaviors by considering the different scaling relations of intrachain and intermolecular hydrogen bonding on the OH content. These results provide insights into the interconnected roles of intra-/intermolecular interactions, polymer chain conformations, and free monomers in solution in affecting polymerization kinetics and dispersion, and point to new opportunities in manipulating polymerization reactions.

INTRODUCTION

Synthetic polymers have widespread applications ranging from fabrics, coatings, and adhesives in our daily lives to advanced optoelectronics and biomimetic materials.[1−7] Making polymers efficiently and with controlled microstructures and even controlled sequences remains a frontier in synthetic chemistry.[8,9] Modulating intra- and intermolecular interactions has been shown to be an effective approach to alter monomer reactivity or bias the polymerization toward the desired reaction pathways.[10−12] Hydrogen bonding (i.e., H-bonding) can tune the electronic properties of methacrylate monomers to increase their reactivity for radical polymerization.[13,14] Intrachain interactions through multidentate coordination of metal ions,[15] bridges made of H-bonding,[16] or templating by bulky chiral groups[17] can facilitate intrachain cyclization instead of interchain cross-linking reactions during radical polymerization of multivinyl monomers.[10] Interactions with the solvent can also impact the outcome of polymerization:[10] poor solvent can induce collapsed chain conformations, facilitating intrachain cyclization,[18] whereas in a good solvent, the excluded volume effect can favor interchain cross-linking reactions.[11]

Recently, we discovered that under living polymerization conditions, single-polymer chains can form *nonequilibrium* conformational entanglements that form and unravel stochastically and that appear to plausibly play key roles in controlling the polymerization kinetics,[19,20] including simple linear polymers such as polynorbornene and polycyclooctene[19] as well as the conjugated polymer polyacetylene for which a

Received: April 7, 2022
Published: June 15, 2022

https://doi.org/10.1021/acscentsci.2c00415
ACS Cent. Sci. 2022, 8, 1116−1124

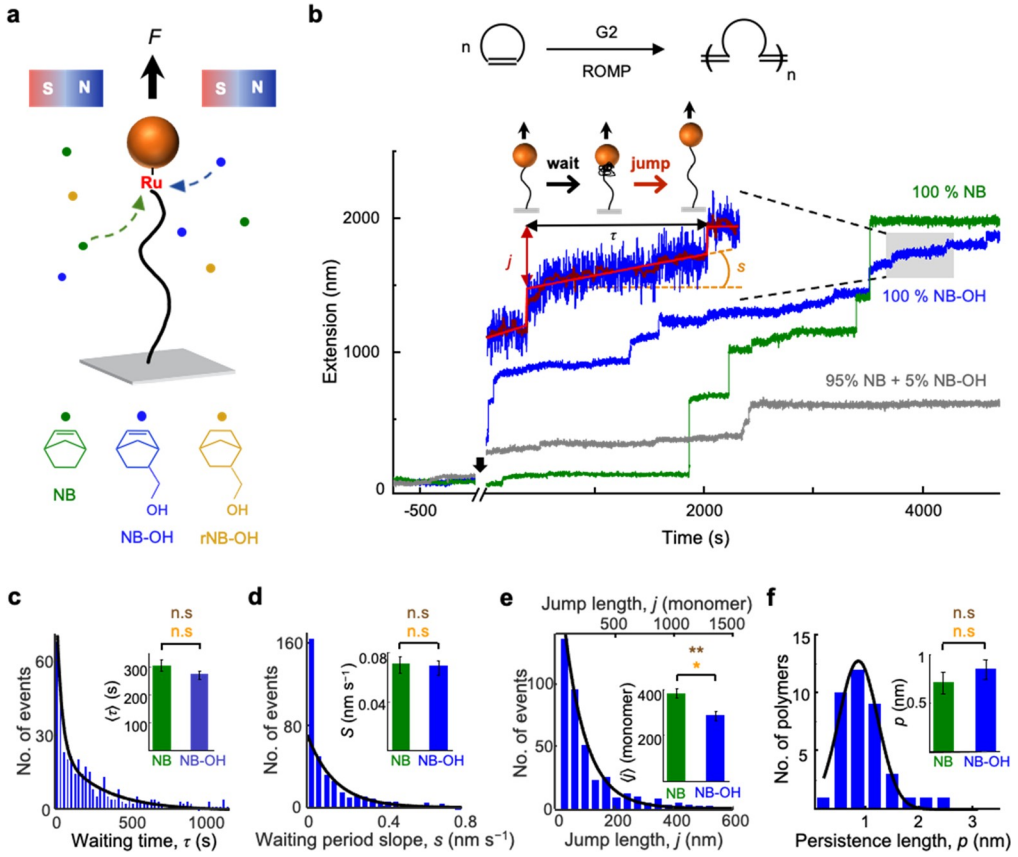

Figure 1. Single-polymer growth measurements using magnetic tweezers. (a) Schematic of magnetic tweezers approach to monitor single-polymer growth during ROMP and of the monomers used in the study. (b) Top: Schematic of ROMP of cyclic olefins catalyzed by second-generation Grubbs catalyst (G2). Bottom: Representative single-polymer extension-vs-time trajectories during the ROMP of 1 M NB-OH (blue trace), 1 M NB (green trace) and 5% NB-OH in a total 1 M NB + NB-OH mixture (gray trace) under a ∼17 pN stretching force. Tether extensions before the monomer addition are shown in a negative time scale. The black arrow marks the monomer addition and flow time during which the extension was not measured. Inset in plot: zoom-in of the gray-boxed region in the blue trace defining the waiting time τ, waiting-period slope s, and jump length j in a single wait-and-jump event. (c–f) Histograms of waiting time, waiting-period slope, jump length, and persistence length of poly(NB-OH). Black lines: double exponential (c), single exponential (d and e), and Gaussian (f) fits; (d) contains an extra population in the first bin of $s \approx 0$ nm s^{-1} for those essentially flat waiting periods, similarly as previously observed for polyNB and polycyclooctene,[19] which is excluded in the fit. Insets: comparisons of τ, s, j, and p averaged over many individual polymers of polyNB and poly(NB-OH). Error bars are SEM. The statistical significance comparing the average values determined using two-sample t test (parametric test, brown fonts) and comparing the distributions using Kruskal–Wallis test (nonparametric test, orange fonts) are represented as * for $P < 0.1$, ** for $P < 0.01$, *** for $P < 0.001$, **** for $P < 0.0001$, and n.s. (nonsignificant) for $P > 0.1$.

monomer ring strain effect is even overruled in forming long chains.[20] There, we used a magnetic tweezers-based approach to monitor single-polymer growth during the ring opening metathesis polymerization (ROMP) of cycloolefins catalyzed by the Ru-based Grubbs second-generation catalyst.[19,20] In this approach (Figure 1a), the growing polymer is tethered between a surface and a magnetic particle, which is pulled by a constant and controllable magnetic force to stretch out the polymer. The linkage to the magnetic particle is via the C═Ru bond of the Ru catalyst, whose *N*-heterocyclic carbene ligand is linked to the particle via alkoxysilane side chains and which is already initiated during the tethering reaction (i.e., its PCy_3 ligand dissociated). During ROMP, the monomers from the surrounding solution are inserted into the C═Ru bond continually, leading to chain propagation and lengthening of the chain's end-to-end extension, which is monitored in real time by following the *z*-position of the magnetic particle. Nevertheless, it is important to note that such single-polymer growth conditions are different from typical bulk polymerization reactions in solution (see also next paragraph), including the pulling force, the tethering of both chain ends, the extreme dilution of polymers, and the polymers formed being from ROMP and being long chains (e.g., many hundreds to thousands of subunits); these conditions might play roles in the formation of the nonequilibrium entanglements.

Many features of this magnetic tweezers experiment distinguish it from polymerization reactions in bulk solution: (1) It directly measures nonequilibrium steady-state kinetics, as there is no monomer depletion (note the monomer-vs-catalyst ratio > 10^7: 1). (2) Long chain lengths up to many thousands of monomers are readily achievable. (3) The kinetics cleanly reflect chain propagation kinetics, as the catalyst is preinitiated. (4) Rebinding of the PCy_3 ligand to the catalyst is negligible, as the ligand is flushed away after the tethering reaction. (5) Interchain interactions are negligible due to the low density of tethered polymers on the surface. It also should be noted that the reaction geometry is analogous to surface-grafted polymer growths,[21−24] except for the presence of the pulling force. This magnetic tweezers approach is part of the emerging efforts toward studying polymerization reactions

https://doi.org/10.1021/acscentsci.2c00415
ACS Cent. Sci. 2022, 8, 1116−1124

of synthetic polymers at the single-molecule level.[19,20,25−29] Bayley et al. have used single-nanopore electrical recording to monitor single poly(disulfide)s polymerization at single-monomer resolution, but the polymer growth was limited to ∼10 subunits by the nanopore size.[26,28] Using single-molecule fluorescence microscopy, Blum et al. visualized the incorporation of single fluorescently labeled monomers into synthetic polymer aggregates amid a high concentration of unlabeled monomers,[27] and Goldsmith et al. have quantified the initiation kinetics of single organometallic catalysts for metathesis polymerization reactions.[30]

The stochastic formation and unraveling of the nonequilibrium conformational entanglements (termed "hairballs") during real-time single-polymer growths were experimentally manifested by the wait-and-jump steps in their extension-vs-time trajectories.[19] The formation of these hairballs likely results from the torsional strains in the backbone that are generated during the polymerization reaction; these hairballs are held together temporarily by intrachain van der Waals interactions, which are broken when they unravel to the thermodynamically equilibrated, extended conformation under force stretching. Furthermore, the properties of these hairballs under such reaction conditions appear to plausibly play key roles in controlling polymerization kinetics, in which those individual polymers having kinetically less stable, structurally looser, and larger hairballs polymerize faster. As the stochastic formation of hairballs makes them naturally dispersed from one polymer to another, they fundamentally contribute to the dispersion of polymerization kinetics and thus dispersion of chain length among individual polymers.

More importantly, the discovery of these hairballs, which are nonequilibrium structures, and of their functional roles immediately points to an unprecedented opportunity to manipulate polymerization kinetics and dispersion: by manipulating the microscopic properties of these hairballs during living polymerization reactions through tuning intramolecular and/or intermolecular interactions. Here, we report a magnetic tweezers study of real-time growth of single polynorbornene-based polymers, in which we systematically tune H-bonding interactions by titrating the OH content in the monomers and the formed polymers during ROMP. This systematic titration is hard to achieve in corresponding bulk experiments due to drastically different and changing solubilities of the monomers and the resulting polymers. Using norbornenes with and without a hydroxyl group and a nonreactive monomer analogue, we show that intrachain and intermolecular H-bonding compete, and both alter the microscopic properties of the nonequilibrium entanglements. The interplay of intra- and intermolecular interactions leads to surprising multiphasic dependences of polymerization dynamics on the OH content in the polymer. We further formulate a simple model to rationalize quantitatively the observed multiphasic behaviors by considering the different scaling relations of intrachain and intermolecular H-bonding on the OH content. These results provide insights into the interconnected roles of intramolecular interactions, intermolecular interactions, polymer chain conformations, and free monomers in affecting polymerization kinetics and dispersion and raise new opportunities to manipulate polymerization reactions.

RESULTS AND DISCUSSION

Intrachain H-Bonding Preserves Conformational Entanglements That Play Key Roles in Single-Chain Polymerization Dynamics. Our approach to manipulate the stability of the nonequilibrium conformational entanglements (i.e., hairballs) is to introduce intrachain H-bonding. We chose H-bonding because it is generally specific to XH functional groups (X = O, N, or F), short in range, and its presence can be turned by controlling the amount of XH groups. We added a CH_2OH group in the norbornene (NB) monomer, i.e., 5-norbornene-2-methanol (NB-OH; Figure 1a; 60:40 *endo*/*exo* mixture; Figure S1). The CH_2OH group of NB-OH is small, rendering minimal structural perturbation to the NB moiety. In a solvent that cannot participate in H-bonding, intrachain H-bonding should be significant, adding stability to the hairballs that form during real-time polymer growth. Furthermore, by mixing the NB and NB-OH monomers in variable ratios, we can modulate progressively the amount of intrachain H-bonding in the resulting copolymer, which should systematically tune the stability of the possible hairballs.

However, even though the second-generation Grubbs catalyst (G2) is known to tolerate OH groups in the monomers,[31,32] the OH group in NB-OH could potentially bind to the catalyst's Ru center, thus impeding the catalysis.[33,34] Therefore, we first measured the real-time single-polymer growth of ROMP with only the NB-OH monomer (1 M) using magnetic tweezers. (All real-time growths were done at a ∼17 pN pulling force under which the equilibrium conformation of semiflexible synthetic polymers follows the worm-like-chain model;[35,36] Figure S2a, and Materials and Methods.) Toluene was used as the solvent. NB-OH monomer is highly soluble in toluene, but the poly(NB-OH) product is not, as confirmed by the polymer precipitations in bulk polymerization reactions (Supporting Information, Section 3). This poor solubility of poly(NB-OH) makes a parallel bulk polymerization experiment impossible but is not an issue in our single-polymer level measurements, which only produce a minuscule amount of polymers (∼picomolar) and in which interchain interactions are negligible. Being able to measure polymers regardless of their solubility is a particular advantage of our experimental approach. This condition of using NB-OH as the only monomer also represents the maximally possible formation of intrachain H-bonds in the polymer, as the solvent is aprotic and if not considering the free monomers in the solution.

To our delight, NB-OH can indeed polymerize via G2-catalyzed ROMP under our experimental conditions. The end-to-end extension of a typical single poly(NB-OH) tethered between a magnetic particle and the coverslip surface increased over time, to hundreds to thousands of nanometers, resulting from the continual insertions of the NB-OH monomer into the Ru═C bond and the accompanying chain propagation, until we flushed out the monomers to terminate the reaction (Figure 1b, blue). This extension-vs-time trajectory exhibits stochastic wait-and-jump steps, characteristic of the probabilistic formation and unraveling of nonequilibrium conformational entanglements (i.e., hairballs) during living polymerization, as observed previously on the growths of single polynorbornene (polyNB) chains (Figure 1b, green) and polycyclooctene.[19] Each wait-and-jump event is associated with one hairball (Figure 1b, inset), whose microscopic properties are characterized by the waiting time (τ), which is

https://doi.org/10.1021/acscentsci.2c00415
ACS Cent. Sci. 2022, 8, 1116−1124

the duration of a hairball and reflects the hairball's kinetic stability; the slope during the waiting period (s), which is a hairball's expansion rate in physical dimension during polymerization and reflects the hairball's global structural looseness; and the jump length (j), which is the chain length newly grown into a hairball and reflects the hairball size. Pooling results from 50 single poly(NB-OH) growth trajectories, the individual waiting times τ follow a double-exponential distribution, averaging at 270 ± 20 s (Figure 1c). Unexpectedly, the average τ, $\langle\tau\rangle$, is only slightly smaller than and almost comparable to the 310 ± 20 s for polyNB grown under the same monomer concentration and pulling force, indicating similar kinetic stabilities between poly(NB-OH) and polyNB hairballs (Figure 1c and inset). The waiting-period slope s mostly follows a single exponential distribution, averaging at 0.07 ± 0.01 nm s^{-1}, which is also unexpectedly undifferentiable from the 0.07 ± 0.01 nm s^{-1} for polyNB, indicating similar structural looseness of their hairballs (Figure 1d and inset). The jump length j follows a single exponential distribution, with an average of 115 ± 6 nm in extension length, corresponding to 290 ± 20 monomers, smaller than the 380 ± 20 monomers for polyNB (Figure 1e and inset).

We further performed force−extension measurements on the individual grown poly(NB-OH) (Methods). They can be satisfactorily fitted by the worm-like-chain model, giving the persistence length (p) and the contour length (L_0) of each polymer[36−39] (Figure S2a). The persistence length follows a normal distribution, with an average of 0.9 ± 0.1 nm, corresponding to ∼1.5 monomers (monomer length ∼0.55 nm, Supporting Information Section 1) and slightly more (rigid) than that of polyNB (0.7 ± 0.1 nm; Figure 1f and inset). The contour length of poly(NB−OH) grown here is in the range of ∼500−4000 nm (Figure S2b), corresponding to ∼900−7300 monomers in length.

The determination of the counter length, in addition to the known total reaction time and monomer length, directly gave the average polymerization rate V (i.e., chain propagation rate) of each polymer. The polymerization rates of individual poly(NB-OH) are heterogeneous, following a log-normal distribution and averaging at 1.9 ± 0.4 monomer s^{-1}, slightly slower than the 2.4 ± 0.4 monomer s^{-1} for polyNB growth under the same reaction conditions (Figure 2a and inset). Furthermore, the polymerization rates of individual polymers show strong negative, positive, and positive correlations, respectively, with their average waiting time, waiting-period slope, and jump length (Figure 2b−d); these observations are consistent with our previous discovery[19,20] that faster polymerizations of individual polymers are associated with hairballs that are kinetically less stable (i.e., shorter average waiting time τ), structurally looser (i.e., larger average slope of the waiting period s), and size-wise larger (i.e., larger average jump length j).

Altogether, these results show that during real-time ROMP in toluene, poly(NB-OH), which is supposed to form extensive intrachain H-bonds, can form nonequilibrium conformational entanglements (i.e., hairballs), and these entanglements still play roles in controlling the polymerization kinetics, despite the polymer's poor solubility. However, even with the supposed intrachain and thus intrahairball H-bonds, the conformational entanglements of poly(NB-OH) do not show significant differences in kinetic stability and structural looseness from those of polyNB (see below further considerations of intermolecular H-bonding between the chain and monomers in the solution).

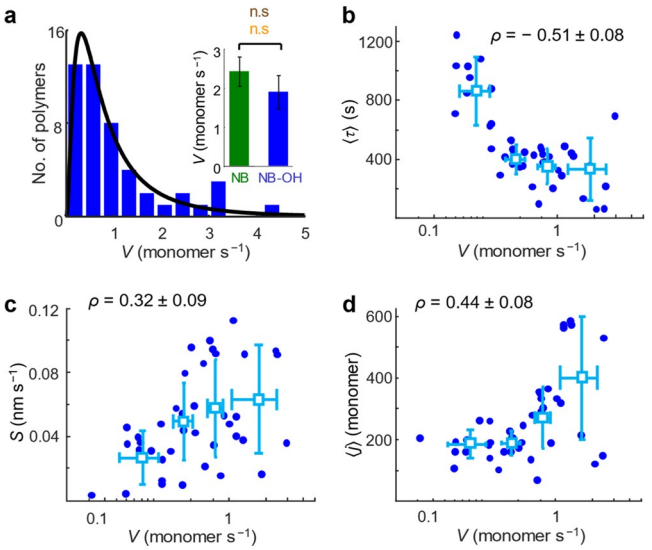

Figure 2. Correlation between polymerization kinetics and hairball properties of single poly(NB-OH) molecules. (a) Distribution of the polymerization rate V of individual poly(NB-OH) molecules. Black line: fit with log-normal distribution: $f(x) = \frac{a}{x}\exp\left(-\frac{(\ln x-\mu)^2}{2\sigma^2}\right)$, where μ is the mean of the logarithmic values, and σ is the standard deviation of the logarithmic values. Inset: comparison of polymerization rates of polyNB and poly(NB-OH) averaged over many individual polymers; error bars are SEM. (b−d) Correlations between an individual polymer's polymerization rate and its average waiting time, waiting-period slope, and jump length for poly(NB-OH). ρ: Pearson's cross correlation coefficient. Each solid blue dot in b−d represents a single polymer; open blue squares are binned and averaged results and the error bars are SD.

Multiphasic Dependences of Single-Polymer Growth Dynamics on Monomer OH Content. To probe why the real-time growth dynamics of single poly(NB-OH) does not differ drastically from those of polyNB and to systematically examine the effects of intrachain H-bonds, we examined the growth of single copolymers of NB and NB-OH, in which we titrated the mole percentage of the NB-OH monomer while keeping the total monomer concentration at 1 M in toluene. At the simplest level, we expect the stabilities of hairballs formed during living polymerization would vary monotonically with increasing OH content in the copolymer backbone. It is worth noting that such systematic titrations in the same solvent are inaccessible for bulk polymerization studies because the solubilities of NB and NB-OH differ significantly, and the solubility of the copolymer is expected to change substantially with increasing OH content, especially for longer chains. These differences and changes in monomer and copolymer solubility would require different solvents at different NB−OH percentages in bulk measurements, whereas solubility is not an issue in our single-polymer level measurements.

For all single copolymer growths and regardless of NB-OH percentages, the real-time extension trajectories maintain the stepwise, wait-and-jump behaviors, reporting hairball formation and unraveling during living polymerization (Figure 1b, gray trajectory, for 5% NB-OH, and Figure S3 for others). Moreover, across all conditions, the polymerization rate V of individual copolymers maintains the correlations with the microscopic properties of their hairballs (Figures S5−S9) like

https://doi.org/10.1021/acscentsci.2c00415
ACS Cent. Sci. 2022, 8, 1116−1124

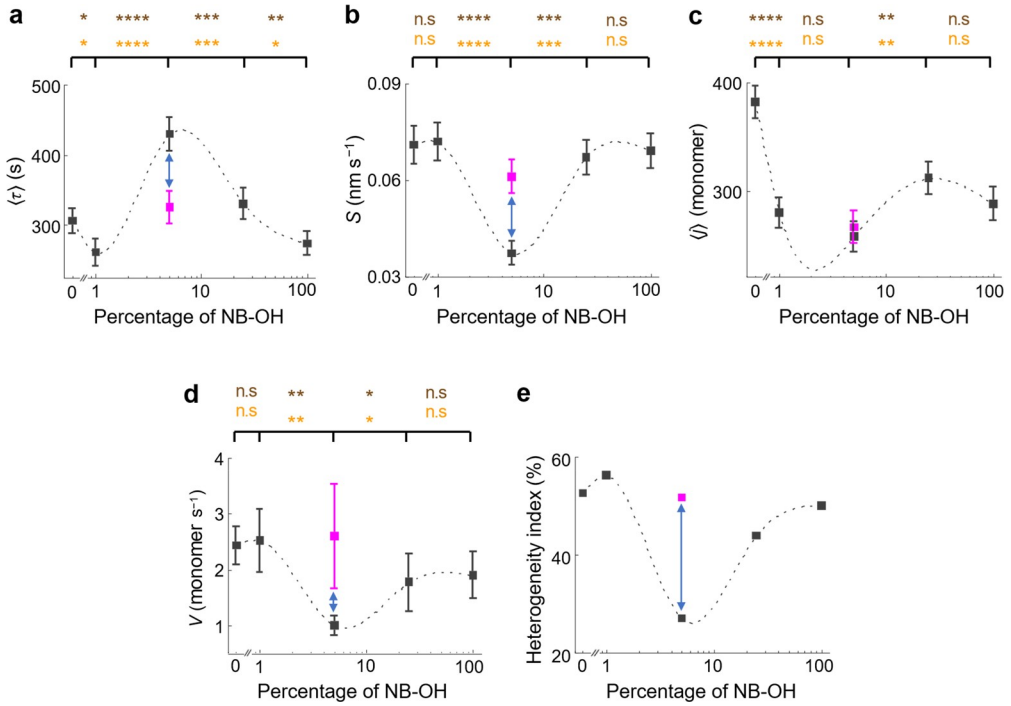

Figure 3. Dependence of single-polymer growth dynamics on monomer OH content. (a–d) Average waiting time, waiting-period-slope, jump length, and polymerization rate of single polymers vs the mole percentage of monomer NB-OH in the total 1 M of NB + NB-OH reactant mixture. Magenta data points are the polymerization condition with 0.2 M rNB-OH added to the 5% NB-OH condition. (e) Heterogeneity index (in percentage), defined as the ratio of standard deviation and the mean (i.e., σ/μ) derived from the log-normal fit of polymerization rate distribution as shown in Figure 2a, vs the NB-OH percentage. The statistical significance comparing the average values determined using two-sample t test (parametric test, brown fonts) and comparing the distributions using Kruskal–Wallis test (nonparametric test, orange fonts) is represented as * for $P < 0.1$, ** for $P < 0.01$, *** for $P < 0.001$, **** for $P < 0.0001$, and n.s. (nonsignificant) for $P > 0.1$.

those in Figure 2b–d. Therefore, the hairballs continue to play key roles in controlling the polymerization kinetics with varying intrachain H-bonding interactions.

However, the average microscopic properties of the hairballs do not change monotonically with increasing NB-OH percentage in the monomers, pooling results from a total of >200 single polymers over five different monomer compositions (Figure 3a–c). The average waiting time, $\langle\tau\rangle$, which reflects the kinetic stability of the hairballs, shows a striking multiphasic dependence with increasing NB-OH percentage: it initially decreases from 0% to 1% NB-OH, and then increases at 5% NB-OH, before it decreases until 100% NB-OH at which its value is comparable to that at 0% NB-OH (Figure 3a). This multiphasic behavior of $\langle\tau\rangle$ indicates that the kinetic stability of hairballs has a complex relation with the percentage of OH groups in the monomers.

Consistently, the average waiting-period slope, S, which reflects the structural looseness of the hairballs, also shows a multiphasic dependence with increasing NB-OH percentage but anticorrelated with that of $\langle\tau\rangle$ (Figure 3b). This anticorrelation is expected because structurally looser hairballs (i.e., larger S) should be kinetically less stable (i.e., shorter $\langle\tau\rangle$). The average jump length, $\langle j\rangle$, which reflects the hairball size, also shows a multiphasic dependence, approximately parallel to that of $\langle\tau\rangle$ (Figure 3c). The consistent appearances of multiphasic behaviors across $\langle\tau\rangle$, S, and $\langle j\rangle$ support that these multiphasic dependences with increasing NB-OH percentages in the monomers indeed reflect actual trends and are not due to indeterminate data variations, even though the titration here only comprises five different ratios in monomer composition. Moreover, this consistency across the three microscopic properties of hairballs strongly suggests a common underlying molecular process that evolves with increasing NB-OH percentage, giving rise to these complex behaviors (see below on mechanism).

As the microscopic properties of hairballs play key roles in controlling the polymerization kinetics under our reaction conditions, their multiphasic dependences on the NB-OH percentage in the monomers should translate into the polymerization rates of individual polymers. Indeed, the average V of individual (co)polymers shows a multiphasic dependence, anticorrelated with that of $\langle\tau\rangle$ but correlated with those of S and $\langle j\rangle$, with increasing NB-OH percentage (Figure 3d). Altogether, these results indicate that tuning the properties of the nonequilibrium conformational entanglements during living polymerization can indeed alter polymerization kinetics, in which complex patterns can translate from one to the other.

We further analyzed the dispersion in polymerization rates of individual (co)polymers. Here, we use a heterogeneity index, which is defined as the standard deviation (σ) divided by the mean (μ) of the log-normal distribution of the polymerization rate V (e.g., Figure 2a) and which quantifies the spread of individual values from their average. Strikingly, the heterogeneity index also shows a multiphasic dependence with increasing NB-OH percentage (Figure 3e), directly correlated with those of the polymerization rate V (Figure 3d). The heterogeneity index-vs-V correlation is somewhat expected, as faster polymerization kinetics typically leads to broader dispersion in linear polymers.[40] The heterogeneity index also shows clear anticorrelation and correlation with the trends of $\langle\tau\rangle$ and S, respectively (Figure 3, panel e vs a,b), supporting

https://doi.org/10.1021/acscentsci.2c00415
ACS Cent. Sci. 2022, 8, 1116–1124

that the properties of conformational entanglements play a key role in the polymer dispersion as well. Analysis of the dispersity gave a similar trend as that of the heterogeneity index (Figure S10).

Role of Intermolecular H-Bonding. The systematic titration of the NB-OH percentage in the monomer mixture revealed unexpected multiphasic behaviors of hairball properties and polymerization kinetics (Figure 3a–d), in sharp contrast to the simplistic prediction that increasing NB-OH percentage should monotonically increase the stability of the hairballs and slow down the polymerization. However, our magnetic tweezers experiments are under real-time living polymerization conditions, in which there are always free monomers present in solution. These free NB-OH monomers should also be able to form H-bonds with the OH group in the growing polymer. Such intermolecular H-bonding would compete with the formation of intrachain H-bonding and potentially destabilize the hairballs. Both intermolecular and intrachain H-bonding would increase with increasing NB-OH percentage during titration, convoluting their respective contributions.

To dissect the effects of intermolecular H-bonding, we introduced 2-norbornanemethanol, the reduced form of NB-OH (i.e., rNB-OH; Figure 1a), along with NB–OH in single-polymer growth experiments. Without a C=C bond, rNB-OH cannot participate in ROMP and thus will only contribute to intermolecular H-bonding with the growing polymer but not to intrachain/intrahairball H-bonding interactions. We chose to add 0.2 M rNB-OH to the 5% NB-OH condition (i.e., 0.05 M NB-OH and 0.95 M NB), where the hairball showed the highest stability, reflected by the longest average waiting time and smallest average waiting-period slope (Figure 3a,b). As such, the total OH group concentration in the solution is 0.25 M, equivalent to that of the 25% NB-OH condition, whereas the percentage of OH in the polymer chain remains the same as that of 5% NB-OH. It should be noted that our experiments are under steady-state polymerization kinetics, where monomer depletion is negligible, and thus the total concentration of OH in the solution remains the same throughout the polymerization process.

In the presence of the added 0.2 M rNB-OH together with 5% NB-OH in solution, the single-polymer growth trajectories still show the wait-and-jump steps (Figure S3). More important, the average waiting time $\langle\tau\rangle$ decreases by about one-fourth compared with the 5% NB-OH condition (Figure 3a, magenta point and blue arrow), indicating a kinetic destabilization of the hairballs by the presence of 0.2 M rNB-OH and consistent with the expected role of the added rNB-OH in contributing only to intermolecular H-bonding. The average waiting-period slope S increases by about two-fifths (Figure 3b, blue arrow), indicating structurally looser hairballs and again supporting rNB-OH's role in forming more intermolecular H-bonds that compete with intrahairball ones. The average jump length $\langle j\rangle$ does not change much (Figure 3c, magenta point). The average polymerization rate V increases by 1.6 times (Figure 3d, blue arrow), even slightly faster than that of the 25% NB-OH condition (Figure 3d), corroborating the idea that kinetically less stable and structurally looser hairballs contribute to faster polymerization kinetics. Consistently, the dispersion of V in the presence of rNB-OH is also larger than those at the 5% and 25% NB-OH conditions (Figure 3e). Taken altogether, these results indicate that the intermolecular H-bonding between free OH in the solution and the OH in the growing polymer chain also play important roles in determining the polymerization kinetics and its dispersion.

Modeling the Interplay between Intrachain and Intermolecular H-Bonding in Affecting Hairball Stability. The experimental results above demonstrated that the stability of the hairball is affected by two competing H-bonding: the intrachain H-bonds stabilize the hairballs, while the intermolecular H-bonds destabilize them (Figure 4a).

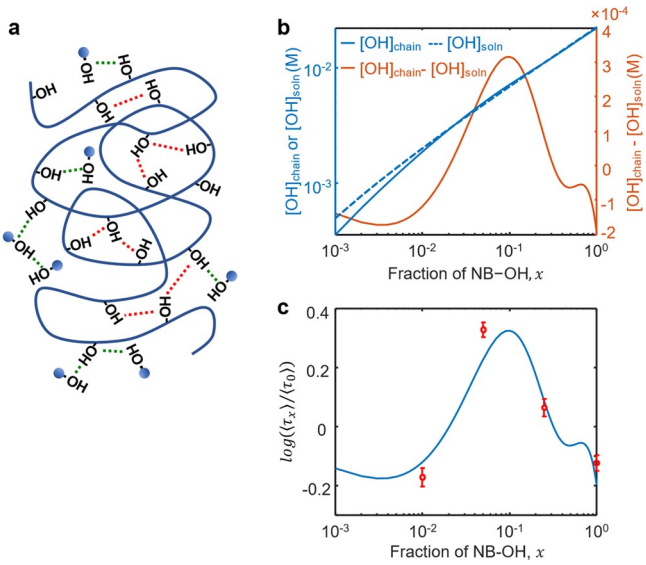

Figure 4. Modeling monomer OH content effect on hairball kinetic stability. (a) Schematic illustration of the intrachain (red) and intermolecular (green) H-bonds. (b) The simulated free OH concentrations in the chain ($[OH]_{chain}$) and in solution ($[OH]_{soln}$) and their difference under different NB-OH mole fractions (x) in a total 1 M monomers. (c) The fitting of relative average waiting time using the model developed in b. $\langle\tau_0\rangle$ is the averaged waiting time in pure NB monomer ($x = 0$), $\langle\tau_x\rangle$ is the averaged waiting time with mixed NB and NB-OH monomers at fraction x. The red open circles are experimental data. Four different functions were tested in our model to empirically account for the steric constraints on the availability of intrachain OH groups; the results shown in b and c use a double-exponential decay function vs x (Figures S16–S17 and Supporting Information, Section 5).

Therefore, the overall stability of the hairballs during real-time polymerization should depend on the probability difference for the incoming NB-OH monomer to form intrachain versus intermolecular H-bonds, which in turn should depend on the concentrations of free OH groups in the growing chain versus in the surrounding solution. The effective concentration of free OH groups in the polymer chain is expected to be dependent on the fraction of the NB-OH monomer in the chain (which is determined by the fraction of NB-OH in the NB + NB-OH monomer mixture) as well as on the chain conformation, which affects not only the effective volume that the intrachain OH groups occupy but also their geometric accessibility. On the other hand, the concentrations of free OH groups in the solution are largely determined by the concentration and thus the fraction of the NB-OH monomer in the monomer mixture. This scaling difference between intrachain and solution free OH groups versus the fraction of the NB-OH monomer likely gives rise to the multiphasic behaviors of hairball stabilities and the associated polymerization kinetics (Figure 3) (see

https://doi.org/10.1021/acscentsci.2c00415
ACS Cent. Sci. 2022, 8, 1116–1124

Supporting Information, Section 4 for rationales *against* the possibility that OH group coordination to Ru is the underlying reason for the observed multiphasic behaviors.)

To quantitatively understand the multiphasic behaviors in Figure 3, we built a simple model to treat the interplay between intrachain and intermolecular H-bond formation (see Supporting Information, Section 5 for detailed model formulation, rationalization, and derivation). Our model takes into account the polymer conformation and the intrachain and intermolecular H-bond formation equilibria. It also considers the steric constraint imposed by the polymer chain on the availability of OH groups in the chains, in which higher percentages of OH groups in the chain decrease the availability of OH groups to form H-bonds. The model also applies the Brønsted linear free energy relationship and Arrhenius equation to relate the energetic stability of hairballs to their kinetic stability that is experimentally manifested by the average waiting time $\langle\tau\rangle$ in the growth trajectories. To simplify the treatment, the model makes the approximations that (1) all H-bonds are energetically equivalent, and (2) each OH group can only form one H-bond regardless of serving as a donor or acceptor because the steric hindrance of the norbornene moiety should impair simultaneous formation of multiple H-bonds around each OH group. (See Supporting Information, Section 5 for the approximations made and discussions on their rationalizations and limitations.)

This model can satisfactorily fit the multiphasic dependence of hairball kinetic stability, as reflected by $\langle\tau\rangle$, versus the fraction of NB-OH in the monomer mixture (Figure 4c), supporting the model's validity. Figure 4b shows the effective concentrations of free OH groups in the chain (i.e., $[OH]_{chain}$) versus the free OH concentration in the solution (i.e., $[OH]_{soln}$) from the fitted results. They show different scaling behaviors versus the fraction of NB-OH in the monomers, as qualitatively described above. More importantly, $[OH]_{chain}-[OH]_{soln}$, which reflects the relative probabilities of forming intrachain versus intermolecular H-bonds, shows the corresponding multiphasic behavior versus the fraction of NB-OH (Figure 4b, orange line). These modeling results directly reflect the complex interplay between intrachain versus intermolecular H-bonding in controlling the hairball stabilities and consequently the polymerization kinetics, in which the decreasing fractional availability of OH in the chain to form H-bonds also plays important roles. More discussions on the fitted results are in Supporting Information, Section 5.

On a separate note, the mere structural perturbation due to the presence of the CH_2OH group in NB-OH is not expected to result in the observed multiphasic dependences of polymerization kinetics. Furthermore, H-bonding is a much stronger interaction in an aprotic solvent, and the observed behaviors are fully interpretable using intra-/intermolecular H-bonding interactions as modeled above. Therefore, H-bonding should play a dominant role in rendering the multiphasic behaviors, while the consequences of structural perturbations and possible changes in other vans der Waals interactions are less significant.

Concluding Remarks. By using magnetic tweezers measurements and titrating H-bonding interactions both intra- and intermolecularly, we have shown that manipulating the stabilities of nonequilibrium conformational entanglements can effectively alter polymerization kinetics and the dispersion of the resulting polymers. The interplay between intra- and intermolecular H-bonding can lead to complex behaviors of polymerization dynamics, in which the conformation of the polymer chain and the free monomers in the solution also contribute substantially. A single-molecule approach here provides advantages in circumventing the challenge of disparate solubilities of the monomer mixtures and the resulting copolymers, making it possible to achieve systematic variations of polymer composition without the need to change the solvent. Besides H-bonding, many other chemical interactions can be incorporated into polymers, such as electrostatic interactions between charged functional groups, metal ion coordination, and $\pi-\pi$ stacking between aromatic groups, to perturb equilibrium or nonequilibrium polymer conformations. The results presented here should help identify more opportunities to manipulate polymerization reactions and understand the molecular basis of their consequences.

METHODS

Materials and Characterization. Norbornene (99%), 5-norbornene-2-methanol (98%, mixture of *endo* and *exo*; *endo*:*exo* ratio of approximately 60:40 as revealed by ^{1}H NMR; Figure S1), 2-norbornanemethanol (97%, mixture of *endo* and *exo* isomers), first-generation Grubbs catalyst (97%), and potassium *tert*-butoxide (reagent grade, ≥98%) were purchased from Sigma-Aldrich and used as received. Alkoxysilane-modified G2 catalyst was synthesized as previously reported.[19] Solvents (Toluene and THF) were dried by passage through solvent purification columns and degassed before use. All manipulations of air- and moisture-sensitive compounds were performed under nitrogen atmosphere in a glovebox or via standard Schlenk line operations. ^{1}H NMR spectra were recorded on an INOVA 600 (600 MHz) spectrometer.

Magnetic Tweezers Experiments and Data Analysis. The details of sample preparation, magnetic tweezers measurements, analysis of single-polymer growth trajectories, and force−extension measurements have been described in our previous studies,[19] and a brief overview is provided in the Supporting Information, Section 1. The reactions were initiated by flowing the monomer solution into the reaction flow cell. The real-time growth was monitored under a constant magnetic stretching force (∼17 pN). Rotational manipulations of the magnetic particle were used to identify single-polymer tethers. The polymerization reaction was stopped by flushing out the monomer solution with pure solvent, after which the force−extension measurements were performed.

Ensemble Polymerization Measurements. The details of ensemble polymerization measurements to complement single-polymer growth measurements are described in detail in the Supporting Information, Section 3.

Data Availability. The raw data that support the findings of this study are available from the corresponding author on reasonable request.

Code Availability. The data analysis algorithm was described in detail in our previous work,[19,20] and the associated MATLAB codes were included in the Supporting Information of our previous publication.[20]

ASSOCIATED CONTENT

Supporting Information

The Supporting Information is available free of charge at https://pubs.acs.org/doi/10.1021/acscentsci.2c00415.

https://doi.org/10.1021/acscentsci.2c00415
ACS Cent. Sci. 2022, 8, 1116−1124

Detailed experimental procedures; additional results and analyses; ensemble polymerization study; detailed quantitative modeling of interplay between intrachain and intermolecular hydrogen bonding in affecting hairball stability (PDF)

Transparent Peer Review report available (PDF)

AUTHOR INFORMATION

Corresponding Authors

Peng Chen − *Department of Chemistry and Chemical Biology, Cornell University, Ithaca, New York 14853, United States;* orcid.org/0000-0001-8582-7661; Email: pc252@cornell.edu

Chunming Liu − *Department of Chemistry and Chemical Biology, Cornell University, Ithaca, New York 14853, United States; Departments of Polymer Science and Chemistry, The University of Akron, Akron, Ohio 44325-3909, United States*; Email: chunmingliu@uakron.edu

Authors

Susil Baral − *Department of Chemistry and Chemical Biology, Cornell University, Ithaca, New York 14853, United States*

Xianwen Mao − *Department of Chemistry and Chemical Biology, Cornell University, Ithaca, New York 14853, United States;* Present Address: Department of Materials Science and Engineering, National University of Singapore, Singapore

Geoffrey W. Coates − *Department of Chemistry and Chemical Biology, Cornell University, Ithaca, New York 14853, United States*

Complete contact information is available at: https://pubs.acs.org/10.1021/acscentsci.2c00415

Author Contributions

[⊥]S.B. and C.L. made an equal contribution. S.B., C.L., and P.C. designed the research. S.B. performed experiments and analyzed the data. C.L. derived the quantitative model and contributed to experiments. X.M. and G.W.C. contributed to discussions. S.B., C.L., and P.C. analyzed results and wrote the manuscript.

Notes

The authors declare no competing financial interest.

ACKNOWLEDGMENTS

We thank K. Kaori for the synthesis of the alkoxysilane-modified *N*-heterocyclic carbene ligand; B. A. Abel and W. You for assistance with glovebox and Schlenk line manipulations; and A. Condo and I. Keresztes for assistance with NMR measurements. The research is supported by the Army Research Office Grant W911NF-18-1-0217. The work made use of the Cornell University NMR facility, which is supported, in part, by the National Science Foundation through MRI Award CHE-1531632, and the Cornell Center for Materials Research Shared Facilities supported by NSF Grant DMR-1719875.

REFERENCES

(1) Pillai, O.; Panchagnula, R. Polymers in Drug Delivery. *Curr. Opin. Chem. Biol.* **2001**, *5*, 447−451.

(2) Green, J. J.; Elisseeff, J. H. Mimicking Biological Functionality with Polymers for Biomedical Applications. *Nature* **2016**, *540*, 386−394.

(3) Samuel, I. D. W.; Turnbull, G. A. Organic Semiconductor Lasers. *Chem. Rev.* **2007**, *107*, 1272−1295.

(4) Ma, H.; Jen, A. K. -Y.; Dalton, L. R. Polymer-Based Optical Waveguides: Materials, Processing, and Devices. *Adv. Mater.* **2002**, *14*, 1339−1365.

(5) Okada, M. Chemical Syntheses of Biodegradable Polymers. *Prog. Polym. Sci.* **2002**, *27*, 87−133.

(6) Burnworth, M.; Tang, L.; Kumpfer, J. R.; Duncan, A. J.; Beyer, F. L.; Fiore, G. L.; Rowan, S. J.; Weder, C. Optically Healable Supramolecular Polymers. *Nature* **2011**, *472*, 334−337.

(7) Ramirez, A. L. B.; Kean, Z. S.; Orlicki, J. A.; Champhekar, M.; Elsakr, S. M.; Krause, W. E.; Craig, S. L. Mechanochemical Strengthening of a Synthetic Polymer in Response to Typically Destructive Shear Forces. *Nat. Chem.* **2013**, *5*, 757−761.

(8) Matyjaszewski, K.; Tsarevsky, N. V. Nanostructured Functional Materials Prepared by Atom Transfer Radical Polymerization. *Nat. Chem.* **2009**, *1*, 276−288.

(9) Domski, G. J.; Rose, J. M.; Coates, G. W.; Bolig, A. D.; Brookhart, M. Living Alkene Polymerization: New Methods for the Precision Synthesis of Polyolefins. *Prog. Polym. Sci.* **2007**, *32*, 30−92.

(10) Gao, Y.; Zhou, D.; Lyu, J.; A, S.; Xu, Q.; Newland, B.; Matyjaszewski, K.; Tai, H.; Wang, W. Complex Polymer Architectures through Free-Radical Polymerization of Multivinyl Monomers. *Nat. Rev. Chem.* **2020**, *4*, 194−212.

(11) Cerid, H.; Okay, O. Minimization of Spatial Inhomogeneity in Polystyrene Gels Formed by Free-Radical Mechanism. *Eur. Polym. J.* **2004**, *40*, 579−587.

(12) Elliott, J. E.; Bowman, C. N. Effects of Solvent Quality during Polymerization on Network Structure of Cross-Linked Methacrylate Copolymers. *J. Phys. Chem. B* **2002**, *106*, 2843−2847.

(13) Siddiqui, M. N.; Achilias, D. S.; Redhwi, H. H. Effect of the Side Ethylene Glycol and Hydroxyl Groups on the Polymerization Kinetics of Oligo(Ethylene Glycol Methacrylates). An Experimental and Modeling Investigation. *Polym. Chem.* **2020**, *11*, 3732−3746.

(14) Schier, J. E. S.; Hutchinson, R. A. The Influence of Hydrogen Bonding on Radical Chain-Growth Parameters for Butyl Methacrylate/2-Hydroxyethyl Acrylate Solution Copolymerization. *Polym. Chem.* **2016**, *7*, 4567−4574.

(15) Terashima, T.; Kawabe, M.; Miyabara, Y.; Yoda, H.; Sawamoto, M. Polymeric Pseudo-Crown Ether for Cation Recognition via Cation Template-Assisted Cyclopolymerization. *Nat. Commun.* **2013**, *4*, 1−9.

(16) Kang, Y.; Lu, A.; Ellington, A.; Jewett, M. C.; O'Reilly, R. K. Effect of Complementary Nucleobase Interactions on the Copolymer Composition of RAFT Copolymerizations. *ACS Macro Lett.* **2013**, *2*, 581−586.

(17) Kakuchi, T.; Narumi, A.; Kaga, H.; Yamauchi, Y.; Obata, M.; Uesaka, T.; Yokota, K. Chirality Induction in Cyclocopolymerization. 14. Template Effect of 1,2-Cycloalkanediol in the Cyclocopolymerization of Bis(4-Vinylbenzoate)s with Styrene. *Macromolecules* **2001**, *34*, 38−43.

(18) Elliott, J. E.; Bowman, C. N. Effects of Solvent Quality during Polymerization on Network Structure of Cross-Linked Methacrylate Copolymers. *J. Phys. Chem. B* **2002**, *106*, 2843−2847.

(19) Liu, C.; Kubo, K.; Wang, E.; Han, K. S.; Yang, F.; Chen, G.; Escobedo, F. A.; Coates, G. W.; Chen, P. Single Polymer Growth Dynamics. *Science* **2017**, *358*, 352−355.

(20) Baral, S.; Liu, C.; Chakraborty, U. K.; Kubo, K.; Mao, X.; Coates, G. W.; Chen, P. Single-Chain Polymerization Dynamics and Conformational Mechanics of Conjugated Polymers. *Chem.* **2021**, *7*, 2175−2189.

(21) Schürer, S. C.; Gessler, S.; Buschmann, N.; Blechert, S. Synthesis and Application of a Permanently Immobilized Olefin-Metathesis Catalyst. *Angew. Chem. Int. Ed* **2000**, *39*, 3898−3901.

(22) Monge-Marcet, A.; Pleixats, R.; Cattoën, X.; Wong Chi Man, M. Sol-Gel Immobilized Hoveyda-Grubbs Complex through the NHC Ligand: A Recyclable Metathesis Catalyst. *J. Mol. Catal. A Chem.* **2012**, *357*, 59−66.

(23) Easter, Q. T.; Trauschke, V.; Blum, S. A. Catalyst Inefficiencies: Supported Ring-Opening Metathesis Polymerization Catalyst Yields

Its Ensemble Rate from a Small Number of Molecular Active Sites. *ACS Catal.* **2015**, *5*, 2290−2295.
(24) Dewaele, A.; Van Berlo, B.; Dijkmans, J.; Jacobs, P. A.; Sels, B. F. Immobilized Grubbs Catalysts on Mesoporous Silica Materials: Insight into Support Characteristics and Their Impact on Catalytic Activity and Product Selectivity. *Catal. Sci. Technol.* **2016**, *6*, 2580−2597.
(25) Liu, C.; Baral, S.; Gu, K.; Mao, X.; Chen, P. Real-Time Single-Polymer Growth towards Single-Monomer Resolution. *Trends Chem.* **2021**, *3*, 318−331.
(26) Shin, S. H.; Bayley, H. Stepwise Growth of a Single Polymer Chain. *J. Am. Chem. Soc.* **2005**, *127*, 10462−10463.
(27) Easter, Q. T.; Blum, S. A. Organic and Organometallic Chemistry at the Single-Molecule, -Particle, and -Molecular-Catalyst-Turnover Level by Fluorescence Microscopy. *Acc. Chem. Res.* **2019**, *52*, 2244−2255.
(28) Pulcu, G. S.; Galenkamp, N. S.; Qing, Y.; Gasparini, G.; Mikhailova, E.; Matile, S.; Bayley, H. Single-Molecule Kinetics of Growth and Degradation of Cell-Penetrating Poly(Disulfide)s. *J. Am. Chem. Soc.* **2019**, *141*, 12444−12447.
(29) Cavell, A. C.; Krasecki, V. K.; Li, G.; Sharma, A.; Sun, H.; Thompson, M. P.; Forman, C. J.; Guo, S. Y.; Hickman, R. J.; Parrish, K. A.; Aspuru-Guzik, A.; Cronin, L.; Gianneschi, N. C.; Goldsmith, R. H. Optical Monitoring of Polymerizations in Droplets with High Temporal Dynamic Range. *Chem. Sci.* **2020**, *11*, 2647−2656.
(30) Ng, J. D.; Upadhyay, S. P.; Marquard, A. N.; Lupo, K. M.; Hinton, D. A.; Padilla, N. A.; Bates, D. M.; Goldsmith, R. H. Single-Molecule Investigation of Initiation Dynamics of an Organometallic Catalyst. *J. Am. Chem. Soc.* **2016**, *138*, 3876−3883.
(31) Bielawski, C. W.; Grubbs, R. H. Highly Efficient Ring-Opening Metathesis Polymerization (ROMP) Using New Ruthenium Catalysts Containing N-Heterocyclic Carbene Ligands. *Angew. Chem., Int. Ed.* **2000**, *39*, 2903−2906.
(32) Sutthasupa, S.; Shiotsuki, M.; Sanda, F. Recent Advances in Ring-Opening Metathesis Polymerization, and Application to Synthesis of Functional Materials. *Polym. J.* **2010**, *42*, 905−915.
(33) Tuba, R.; Al-Hashimi, M.; Bazzi, H. S.; Grubbs, R. H. One-Pot Synthesis of Poly(Vinyl Alcohol) (PVA) Copolymers via Ruthenium Catalyzed Equilibrium Ring-Opening Metathesis Polymerization of Hydroxyl Functionalized Cyclopentene. *Macromolecules* **2014**, *47*, 8190−8195.
(34) Al-Hashimi, M.; Tuba, R.; Bazzi, H. S.; Grubbs, R. H. Synthesis of Polypentenamer and Poly(Vinyl Alcohol) with a Phase-Separable Polyisobutylene-Supported Second-Generation Hoveyda-Grubbs Catalyst. *ChemCatChem.* **2016**, *8*, 228−233.
(35) Bouchiat, C.; Wang, M. D.; Allemand, J. F.; Strick, T.; Block, S. M.; Croquette, V. Estimating the Persistence Length of a Worm-like Chain Molecule from Force-Extension Measurements. *Biophys. J.* **1999**, *76*, 409−413.
(36) Dittmore, A.; McIntosh, D. B.; Halliday, S.; Saleh, O. A. Single-Molecule Elasticity Measurements of the Onset of Excluded Volume in Poly(Ethylene Glycol). *Phys. Rev. Lett.* **2011**, *107*, 148301.
(37) Saleh, O. A. Perspective: Single Polymer Mechanics across the Force Regimes. *J. Chem. Phys.* **2015**, *142*, 194902.
(38) Latinwo, F.; Schroeder, C. M. Model Systems for Single Molecule Polymer Dynamics. *Soft Matter* **2011**, *7*, 7907−7913.
(39) Schroeder, C. M. Single Polymer Dynamics for Molecular Rheology. *J. Rheol.* **2018**, *62*, 371.
(40) Odian, G. *Principles of Polymerization*; John Wiley & Sons, 2004.

https://doi.org/10.1021/acscentsci.2c00415
ACS Cent. Sci. 2022, 8, 1116−1124